17th Australasian Fluid Mechanics Conference
Auckland, New Zealand
5-9 December 2010

Effect of Surface Roughness on Small-Scale Velocity and Scalar Characteristics in a Turbulent Channel Flow

P. Orlandi[1], R.A. Antonia[2] and S. Leonardi[3]

[1] Dipartimento di Meccanica e Aeronautica,
Universita La Sapienza, 00184 Rome, Italy

[2] School of Engineering, University of Newcastle, NSW 2308, Australia

[3]Department of Mechanical Engineering
University of Puerto Rico, Mayaguez, 00680 Puerto Rico US

Abstract

Using DNS data in a turbulent channel flow, the paper examines the effect of the surface geometry on the vorticity and (passive) scalar gradient vectors at a relatively small Reynolds number and for a molecular Prandtl number of 1. While a strong correlation between these two vector fields is expected close to the wall when the latter is smooth, significant changes occur when the surface is modified by roughness elements. Different shaped elements, placed orthogonally to the flow with a small streamwise spacing, are considered. The largest and smallest disturbances occur for triangular and square elements respectively whereas the disturbance from circular elements is intermediate to that of the previous two geometries. This result is reflected in nearly all the small-scale statistics that have been obtained, including correlations between components of the vorticity and scalar gradient vectors. Local isotropy near the wall is more closely approximated for the triangular elements.

Introduction

A ubiquitous feature of a turbulent flow in the vicinity of a smooth wall is the presence of quasi-streamwise vortices and their associated low and high-speed streaks. When a passive scalar is introduced in the flow, e.g. by slightly heating either the flow or the wall, the close correspondence between velocity and thermal streaks translates into a nearly perfect correlation, close to the surface, between the longitudinal velocity fluctuation u_1 and the scalar fluctuation θ ,e.g. Iritani *et al.* [7], Antonia *et al.*[2], Kim and Moin [8]. This is in turn reflected in strong correlations between some of the components of the vorticity vector and those of the scalar gradient vector. In particular, there is a strong correlation between either ω_3 (the spanwise vorticity fluctuation) and $\theta_{,2}$ ($\equiv \partial\theta/\partial x_2$,the derivative of θ along the wall- normal direction x_2) or ω_2 (the wall-normal vorticity fluctuation) and $\theta_{,3}$ ($\equiv \partial\theta/\partial x_3$ the derivative of θ along the spanwise direction x_3) (Abe *et al.* [1]). The latter authors found that the maximum correlation coefficient associated with the previous pairs of quantities is very close to either +1 or -1 and emphasized that these small-scale related quantities can provide more accurate statistics for the velocity and thermal streaks than u_1 and θ.

Since the quasi-streamwise vortices are by and large responsible for transporting momentum and heat near a smooth wall, it is important to understand how these vortices are affected by modifications to the surface in view of the obvious practical implications this has for managing turbulent wall flows. More basically, the streaks are no longer observed when the surface is sufficiently rough so that it may be argued that a study of rough-wall layers can help us, albeit indirectly, to better appreciate the role of the viscous layer as well as the importance of the streaks.

An earlier paper (Orlandi *et al.* [15]) considered the effect of 2D roughness elements, with various geometries, placed either along the flow direction or orthogonally to it on one of the walls of a turbulent channel flow, the opposite wall being kept smooth. For orthogonal elements, no satisfactory correlation could be found between the Hama roughness function and any of the usual parameters used for describing the roughness. On the other hand, a satisfactory collapse of the DNS data was obtained by plotting the roughness function in terms of the rms wall-normal velocity, averaged over the plane of the roughness crests. Since the modifications to the wall-normal velocity fluctuation u_2 are most likely caused by changes to the vortical structures in the vicinity of the elements, it seemed natural to extend the previous work by investigating how the roughness geometry affects the fluctuating vorticity vector and also, in the context of our earlier comments regarding the advantages of introducing a passive scalar in the flow, its relationship with the fluctuating scalar gradient vector.

In this paper, we focus only on orthogonal (drag-augmenting) elements with a streamwise spacing w that is comparable to the height k of the roughness elements and provide conventional statistics for these two vectors as well as for the non-zero components of the vorticity-scalar gradient tensor. Given that the two vectors reflect, to a large extent, small-scale characteristics of the turbulence, the statistics also provide a means of testing the approach towards local isotropy when the surface geometry is altered; this is of some interest in the context of modelling, especially in view of the strong anisotropy of the scalar gradient vector near a smooth wall [10]. We consider circular, square and triangular elements (see figure 1) of height k =0.2 h (h is the channel half-width). In each case, the ratio w/k is 1 so that the corresponding magnitude of the roughness function is small compared to its maximum value, which occurs typically when w/k is near 7 (Leonardi *et al.*[11]).

Numerical Procedure

A detailed description of the numerical method has been given in [13]. Only the salient aspects are recalled here briefly. The incompressible Navier-Stokes and energy equations are discretised in an orthogonal coordinate system using the staggered central second-order finite difference approximation. The discretised system is advanced in time using a fractional step method with viscous terms treated implicitly and convective terms explicitly. The large sparse matrix resulting from the implicit terms is inverted with an approximate factorization

technique. At each time step, the momentum equations are advanced with the pressure at the previous step, yielding an intermediate non-solenoidal velocity field which is subsequently projected onto a solenoidal one. A hybrid third-order Runge Kutta scheme is used to advance the equations in time. The roughness is treated by the efficient immersed boundary technique[5,15,16].This allows flows over complex geometries to be solved whilst avoiding computationally-intensive body fitted grids; the approach can handle flows above any kind of surface, albeit by clustering a large number of points near the elements.

The computational box is $8h$ in the streamwise (x_1), $2.2h$ in the wall-normal (x_2) and πh in the spanwise (x_3) directions with a grid of 400 x 158 x 128. Each roughness element (of height $0.2h$) is described by a 10 x 30 grid. For the smooth wall channel flow, the Reynolds number Re, based on U_P (the Poiseuille centre line velocity), is 4200; this corresponds to $h^+ \approx 180$. No heat sources are added to the temperature transport equation so that the total heat flux is approximately constant across the channel when steady state is reached; the temperature is assigned a value (normalized by the temperature on the upper wall) of +1 at the lower rough wall and -1 at the upper smooth wall. The molecular Prandtl number Pr ($\equiv \nu/\kappa$; ν and κ are the momentum and thermal diffusivities respectively) is set equal to 1. The coordinate system is such that the origin (x_2) is at the centre of the channel. The roughness is placed on the bottom wall ($x_2 = -1.2h$) with the plane of the crests at $x_2 = -h$. The upper wall ($x_2 = +h$) is smooth. The friction velocity on the rough wall is determined from the sum of the pressure integral around the roughness elements and the local shear stress on the surface[10]. An experimental validation of the simulation was reported by Burattini *et al.* [3], albeit for one roughness geometry (square elements, with $k = 0.1\ h$ and $w/k = 3$) and three values of Re. In each case, reasonably good agreement was found for the mean velocity and Reynolds stress profiles as well as spectra and integral length scales of all three velocity fluctuations.

Results

A measure of the disturbance introduced by the roughness elements is given by the rms pressure distributions across the channel. These distributions (not shown here) indicate that the maximum rms pressure occurs at $x_2 = 0$, at the roughness crest (over a smooth surface , it occurs at $x_2+ \approx 30$, as reported by Kim *et al.*[9]). Relative to the smooth wall peak value, the peak rms pressure over the roughness is significantly larger , by factors of almost 2, 6 and 7 for the square, circular and triangular elements respectively. The variation in the level of disturbance between these 3 geometries is illustrated via the instantaneous wall-normal vorticity contours of Fig 1. For the square elements, the contours are somewhat elongated and resemble those over the smooth wall, alternating in sign along the spanwise direction. This particular geometry has been traditionally described as a 'd-type' roughness, see e.g. [17,4,13].The vortical streaks are shorter and more steeply inclined to the wall for the circular elements. The inclination is increased further for the triangular elements. Although w/k is only 1, the ω_2 contours over the triangular elements are not dissimilar to those presented by Leonardi et al. [12] and Ikeda & Durbin [6] for square elements but with a value of w/k that is close to that for which the drag is near its maximum value. One implication of the break-up and loss of preferred orientation of the quasi-streamwise vortices by the roughness is that the vorticity and scalar gradient concentrations become more evenly distributed between the x_1 , x_2 and x_3 directions, thus indicating that the isotropic relations

$$< \omega_1^2 >=< \omega_2^2 >=< \omega^2_3 > \quad \text{.... (1)}$$

and

$$< \theta_{,1}^2 >=< \theta_{,2}^2 >=< \theta_{,3}^2 > \quad \text{.... (2)}$$

should be more closely approximated over the triangular and circular elements than the square elements or the smooth wall (the angular brackets denote averaging with respect to x_1 , x_3 and t).

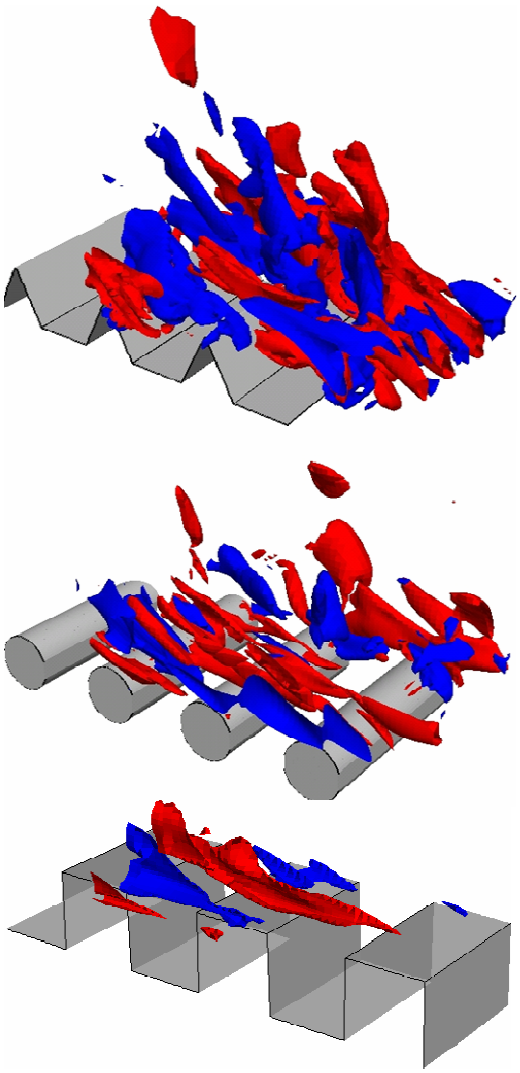

Figure 1 Instantaneous wall-normal vorticity contours $\omega_2 = \pm 3$. *The red and blue contours refer to positive and negative* ω_2 *respectively.*

Figure 2 shows that this is indeed the case as the ratios $\theta'_{,1} / \theta'_{,2}$ (figure 2a) and $\theta'_{,1} / \theta'_{,3}$ (figure 2b) (the prime denotes the rms value) are closer to 1 for the triangular elements. For the circular elements, these ratios lie between those for the other two geometries. All three rms values (for both scalar derivative and

vorticity components) increase as the geometry changes between square, circular and triangular shapes. This increase means that the mean enstrophy (effectively the mean energy dissipation rate) and mean scalar dissipation rate also increase accordingly. Note however that the rms values of the lateral scalar derivatives increase almost similarly among the three elements so that the distribution of $\theta'_{,2}/\theta'_{,3}$ (figure 2c) is basically unchanged. This latter ratio increases to almost 2 at the roughness crest plane, implying that local axisymmetry is not significantly improved by the roughness. A small but discernible variation exists for $\omega'_{,2}/\omega'_{,3}$ (figure 2f), the distribution over the triangular elements being closer to 1. Overall, the distributions of figures 2d, e, f indicate that local isotropy is more closely approximated by the vorticity vector than the scalar derivative vector, due mainly to a stronger increase, relative to the lateral components, in the rms streamwise vorticity than in $\theta'_{,1}$. Nevertheless, one cannot ignore the major improvement in the local isotropy of the scalar gradient vector as a result of changes in the surface geometry. For example, the maximum value of $\theta'_{,2}/\theta'_{,1}$ is reduced from about 6.2 (square elements) to 2.6 (triangular elements) ; at the same x_2/h, this ratio is close to 25 over the smooth wall.

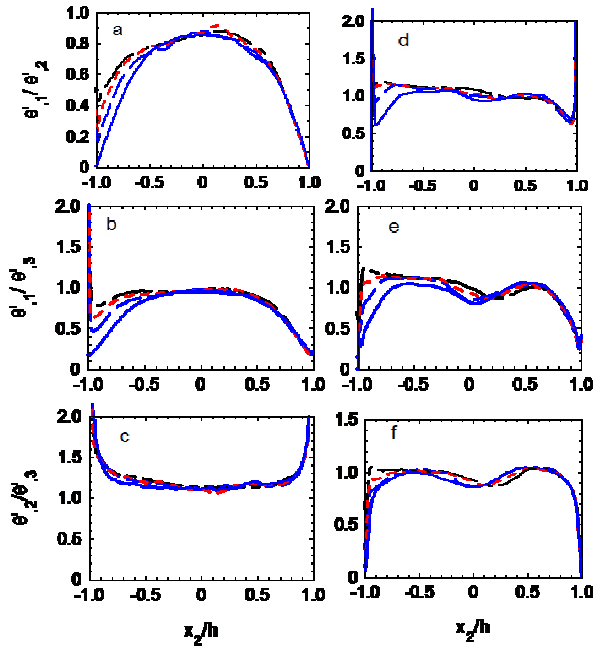

Figure 2 Ratios of rms scalar gradient and lateral vorticity components. The solid (blue), dashed (blue), dotted (red), dash-dotted (black) lines refer to the smooth wall , and the square, circular and triangular elements respectively.

The correlation tensor $<\omega_i\theta_j>$ has four non-zero components : $<\omega_2\theta_3>$, $<\omega_3\theta_2>$, $<\omega_1\theta_3>$ and $<\omega_3\theta_1>$, the remaining five components being zero by virtue of symmetry about x_3. Smooth wall DNS data [1] have indicated that the correlation coefficients associated with the first two quantities reach a magnitude close to unity as the wall is approached. Figure 3 shows that the maximum magnitude of the correlation coefficient (defined as $\rho_{\alpha,\beta} = <\alpha\beta>/\alpha'\beta'$) between either ω_2 and θ_3 (figure 3a) or ω_3 and θ_2 (figure 1b) indeed approaches 1 on the smooth wall. This magnitude is however significantly reduced (by nearly a factor of 2) for the triangular elements; it is less affected for the square elements. This reduction is not surprising in the light of the previous observations and results of figure 2. Note that the effect of the surface roughness geometry extends well beyond the channel centre line, especially in the case of the circular and triangular elements. As expected, all the four distributions become indistinguishable near the upper (smooth) channel wall. The distribution of $\rho_{u_1\theta}$ (not shown here) is similar to that of $\rho_{\omega_2\theta_2}$ near the lower wall and also, allowing for the change of sign, to that of $\rho_{\omega_2\theta_3}$. This result simply reflects the expected relatively strong correlation along streak boundaries between the gradients, with respect to either x_2 or x_3, of u_1 and those of θ.

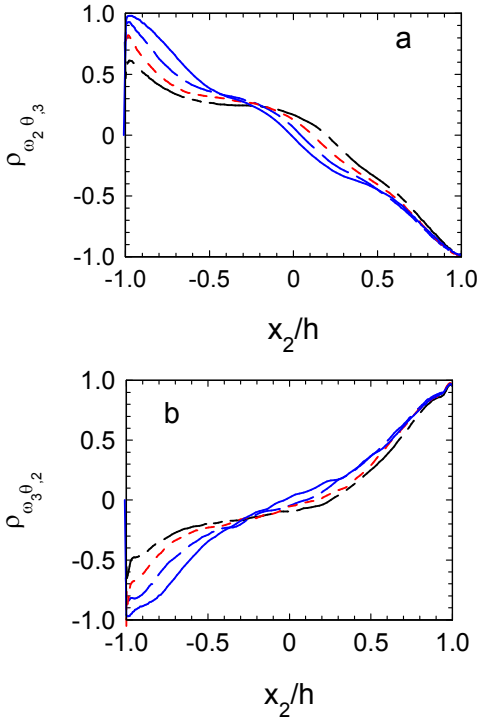

Figure 3 Correlation coefficients between ω2 and θ3 (a) or ω3 and θ2 (b). Line types are as in figure 2.

The peak values of the correlation coefficients associated with the pairs (ω_1 and θ_3) (figure 4a) and (ω_3 and θ_1) (figure 4b) are significantly smaller by comparison to those in figure 3. The former has a peak value of 0.25 near the wall and is somewhat less affected by the roughness change than the latter. Near the smooth wall, $<\omega_1\theta_3>$ changes sign (increases from about -0.25 to about +0.25) due to the motion $\rho_{\omega_2\theta_3}$ induced by the non-slip boundary condition at the wall, e.g.[9,1]). This change in sign is also observed in the distribution (not shown here) of $<\omega_1\omega_2>$. The sign change is however no longer evident with either the cylindrical or triangular elements, the distributions of $<\omega_1\theta_3>$ and $<\omega_1\omega_2>$ remaining positive throughout the channel. Whilst the streaks remain attached over the square cavities, thus allowing for a sign reversal in ω_1, attachment is much less likely (e.g. figure 1) for the other two surfaces.

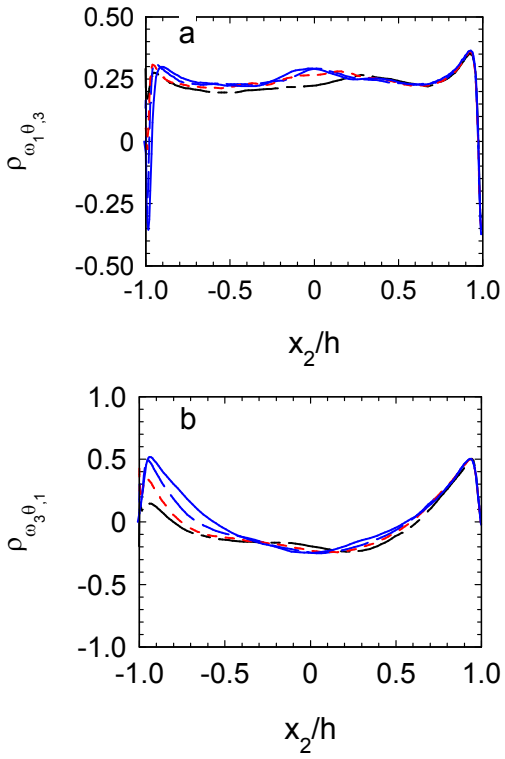

Figure 4 Correlation coefficients between ω1 and θ_3 (a) or ω3 and θ_1 (b). Line types are as in figure 2.

Conclusions

The present results indicate that the vortical motion, which is relatively well organised near a smooth wall, can become severely disorganized depending on the modification that is made to the surface. In this paper, the modification was brought about by the introduction of square, cylindrical and triangular elements aligned along the spanwise direction with a streamwise spacing equal to the height of the element. A passive scalar was also used to highlight the level of the disruption arising from the surface modification. While only minor changes, relative to the smooth wall case, were observed to the vorticity and scalar gradient vectors for the square elements, major changes occurred for the cylindrical and ,more especially, the triangular elements. These changes resulted in the vorticity vector and, to a smaller extent, the scalar gradient vector becoming more isotropic. The correlation between the lateral vorticity and scalar gradient components, which is almost perfect in the vicinity of a smooth wall is significantly reduced over the circular and, in particular, the triangular elements.

Acknowledgments

PO acknowledges the support of MIUR and MURST – RAA is grateful for the support of the ARC – SL acknowledges the National Science Foundation through TeraGrid resources provided by SDSC and TACC.

References

[1] Abe, H., Antonia, R.A. & Kawamura, H. Correlation between Small-Scale Velocity and Scalar Fluctuations in a Turbulent Channel Flow, *J. Fluid Mech.*, **627**, 2009, 1-32.

[2] Antonia, R.A., Krishnamoorthy, L.V. & Fulachier, L. Correlation between the Longitudinal Velocity Fluctuation and Temperature Fluctuation in the Near-Wall Region of a Turbulent Boundary Layer, *Int. J. Heat Mass Transfer* **31**, 1988, 723-730.

[3] Burattini, P., Leonardi, S., Orlandi. P. & Antonia, R.A. Comparison between Experiments and Direct Numerical Simulations in a Channel Flow with Roughness on one Wall, *J. Fluid Mech.* **600**, 2008, 403-426.

[4] Djenidi, L. Elavarasan, R. & Antonia, R.A. The Turbulent Boundary Layer with Square Cavities, *J. Fluid Mech.*, **395**, 1999, 271-294.

[5] Fadlun, E. A., Verzicco, R., Orlandi, P. & Mohd- Yusof, J. Combined Immersed Boundary Finite- Difference Methods for Three- Dimensional Complex Flow Simulations, *J. Comput. Phys.*, 161, 2000, 35-60.

[6] Ikeda, T. & Durbin. P. A., Direct Simulations of a Rough-Wall Channel Flow , *J. Fluid Mech.*, **571**, 2007, 253-263.

[7] Iritani, Y., Kasagi, N. & Hirata, M Heat Transfer Mechanism and Associated Turbulence Structure in the Near-Wall region of a Turbulent Boundary Layer. In *Turbulent Shear Flows* **4** (eds. L.J.S. Bradbury, F. Durst, B.E. Launder, F.W. Schmidt and J.H. Whitelaw), pp 223-234, Springer, 1985.

[8] Kim, J. & Moin, P. Transport of Passive Scalars in a Turbulent Shear Flow In *Turbulent Shear Flows* **6** (eds. J-C Andre, J. Cousteix, F. Durst, B.E. Launder, F.W. Schmidt and J.H. Whitelaw) pp 85-96, Springer, 1989.

[9] Kim, J., Moin, P. & Moser, R. Turbulence Statistics in Fully Developed Channel Flow at Low Reynolds Number, *J. Fluid Mech.*, **177**, 1987, 133-166.

[10] Krishnamoorthy, L.V. & Antonia, R..A. Temperature Dissipation Measurements in a Turbulent Boundary Layer *J. Fluid Mech.***176**, 1987, 265-281.

[11] Leonardi, S., Orlandi, P., Smalley, R.J., Djenidi, L. & Antonia, R.A. Direct Numerical Simulations of Turbulent Channel Flow with Transverse Square Bars on the Wall, *J. Fluid Mech.*, **491**, 2003, 229-238.

[12] Leonardi, S, Orlandi, P., Djenidi, L. and Antonia, R.A. Structure of Turbulent Channel Flow with Square Bars on one Wall, *Int. J. Heat Fluid Flow*, **25**, 2004, 384-392.

[13] Leonardi, S., Orlandi, P. & Antonia, R.A. Properties of d- and k-type Roughness in a Turbulent Channel Flow, *Phys. Fluids*, 19, **2007**, 125101.

[14] Orlandi, P. *Fluid Flow Phenomena: A Numerical Toolkit*, Kluwer, 2000.

[15] Orlandi,P. & Leonardi, S. DNS of Turbulent Channel Flow with Two- and Three-Dimensional Roughness, *J. Turbulence*, **7**, 2006, 1-22.

[16] Orlandi, P., Leonardi, S. & Antonia, R. A., Turbulent Channel Flow with either Transverse or Longitudinal Roughness Elements on one Wall, *J. Fluid Mech.*, **561**, 2006, 279-305.

[17] Perry, A.E., Schofield, W.H. & Joubert, P.N. Rough Wall Turbulent Boundary Layers, *J. Fluid Mech.*, **37**, 1969, 383-413.